

---

## RUBRIKA

---

# A Hybrid Material Based on Poly-3-Amine-7-Methylamine-2-Methylphenazine and Magnetite Nanoparticles

S. Zh. Ozkan<sup>a\*</sup>, G. P. Karpacheva<sup>a</sup>, P. A. Chernavskii<sup>b</sup>, E. L. Dzidziguri<sup>c</sup>,  
G. N. Bondarenko<sup>a</sup>, and G. V. Pankina<sup>b</sup>

<sup>a</sup> Topchiev Institute of Petrochemical Synthesis, Russian Academy of Sciences, Moscow, 119991 Russia

<sup>b</sup> Faculty of Chemistry, Moscow State University, Moscow, 119991 Russia

<sup>c</sup> National University of Science and Technology "MISIS", Moscow, 119049 Russia

\*e-mail: ozkan@ips.ac.ru

Received May 10, 2018; in final form, May 16, 2018

**Abstract**—For the first time, under the conditions of in situ oxidative polymerization, a hybrid dispersed magnetic material based on poly-3-amine-7-methylamine-2-methylphenazine (PAMMPh) is obtained in which nanoparticles  $\text{Fe}_3\text{O}_4$  are dispersed in an electroactive polymer matrix. According to the results of TEM and SEM,  $\text{Fe}_3\text{O}_4$  nanoparticles have sizes of  $4 < d < 11$  nm. Using IR spectroscopy it is established that the chain propagation proceeds via the addition of C—N between 3-amino groups and the *para* position of phenyl rings relative to nitrogen. The chemical structure, phase composition, and the magnetic and thermal properties of the nanomaterials versus the synthetic conditions are investigated. It is shown that the nanocomposite material  $\text{Fe}_3\text{O}_4/\text{PAMMPh}$  is superparamagnetic and thermally stable.

**DOI:** 10.1134/S1995078018020064

## INTRODUCTION

New-generation materials with enhanced functional characteristics are hybrid metal–polymer nanocomposites including polymers with a conjugated system and capable of exhibiting excellent electrical, optical, magnetic, and electrochemical properties. In this class of hybrid materials, a special place is occupied by magnetic nanocomposites. [1–3]. Functional properties of such nanocomposites are determined by both the nature of magnetic nanoparticles and the specific electronic structure of a polyconjugated system, providing a combination of magnetic, electrical, electrochemical, and other useful properties. Interest in such materials is growing, which is evidenced by a great stream of scientific literature devoted to different aspects of the creation and investigation of hybrid nanomaterials.

The most efficient technique of obtaining hybrid nanocomposites is the in situ oxidative polymerization of monomers in the reaction medium containing magnetic nanoparticles [4–20]. Such hybrid nanomaterials are superparamagnets due to the small sizes and high degree of dispersion of magnetic nanoparticles. Thanks to the combination of electrical and magnetic properties, such hybrid nanomaterials are rather attractive for modern technologies. Therefore, the issues of designing new nanocomposite materials based on polyconjugated systems and magnetic nanoparticles are urgent. They can be applied in mag-

netic data-recording systems; as antistatic coatings and materials absorbing electromagnetic radiation in different wavelength ranges; for obtaining anticorrosive coatings; in the creation of components of electronic engineering, electromagnetic screens, and contrast materials for magnetic resonance tomography; in hyperthermia; and for catalytic removal of organic water pollutants in combination with magnetic separation for water purification.

Earlier we obtained a nanostructured magnetic material based on polydiphenylamine-2-carboxylic acid (PDPHAC) and  $\text{Fe}_3\text{O}_4$  nanoparticles by means of the oxidative polymerization of diphenylamine-2-carboxylic acid under homogeneous and interfacial conditions [21–23]. Superparamagnetic materials are also obtained on the basis of polyphenoxazine (PPhOA) [24] and magnetite nanoparticles. Regardless of the synthesis technique, the resulting hybrid nanomaterials are superparamagnets. The squareness ratio of the hysteresis loop  $k_s = M_R/M_S \sim 0$  is evidence of a nearly 100% content of superparamagnetic nanoparticles. The saturation magnetization  $M_S$  increases with an increase in the content of  $\text{Fe}_3\text{O}_4$  nanoparticles and reaches 33.5 and 49.2 emu/g for nanocomposites including PDPHAC and PPhOA, respectively.

In the present work, for the first time, a hybrid dispersed magnetic material based on thermally stable electroactive poly-3-amine-7-methylamine-2-methylphenazine (PAMMPh) and magnetite nanopar-

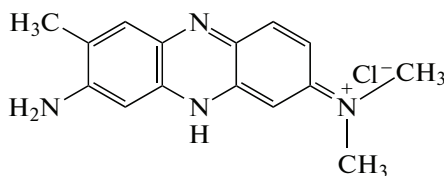
**Table 1.** Magnetic characteristics of the  $\text{Fe}_3\text{O}_4/\text{PAMMPh}$  nanocomposite

Fe, %*	$H_C$ , Oe	$M_S$ , emu/g	$M_R$ , emu/g	$M_R/M_S$
21.2	0	16.26	0	0
33.5	1	31.52	0.2	0.006
44.5	3.5	34.97	0.25	0.007
50.4	0	55.65	0	0

\*According to AAS data.  $H_C$  is the coercive force,  $M_S$  is the saturation magnetization, and  $M_R$  is the residual magnetization.

ticles is obtained. The nanocomposite material  $\text{Fe}_3\text{O}_4/\text{PAMMPh}$  is characterized by Fourier transform IR spectroscopy (FTIR), X-ray phase analysis (XRA) and X-ray structural analysis (XSA), transmission (TEM) and scanning electron microscopy (FE-SEM), atomic absorption spectrometry (AAS), differential scanning calorimetry (DSC), thermogravimetric analysis (TGA), and magnetometry. The chemical structure and phase composition and the magnetic and thermal properties of the obtained nanomaterials versus the synthetic conditions are investigated.

For the synthesis of the nanocomposite, 3-amine-7-dimethylamine-2-methylphenazine hydrochloride (ADMPhH) (Neutral Red)



was taken as a monomer. The presence of two phenyl rings and active functional groups in the ADMPhH chemical structure, which are capable of further transformations, makes it possible to obtain a new type of heterocyclic polyconjugated systems with practically important properties (e.g., high thermal stability and electroactivity in a wide pH range and the ability to yield film coatings in the course of synthesis at the surface of a substrate introduced into the reaction solution) [25].

## EXPERIMENTAL

Analytical-reagent grade ammonium persulfate was refined by recrystallization from distilled water using a well-known technique [26]. 3-Amine-7-dimethylamine-2-methylphenazine hydrochloride ( $C_{15}H_{17}\text{ClN}_4$ ) (ADMPhH) (Neutral Red), as well as iron (II) chloride, acetonitrile, and DMFA (all produced by Acros Organics); iron (III) chloride (pure grade); and ammonia water (reagent grade) were used with no extra purification. Aqueous solutions of the reagents were prepared with distilled water. Poly-3-amine-7-dimethylamine-2-methylphenazine (PAMMPh)

was obtained under the conditions of in situ chemical oxidative polymerization in an acetonitrile aqueous solution [25].

The  $\text{Fe}_3\text{O}_4/\text{PAMMPh}$  nanocomposite was obtained as follows [27]. Firstly,  $\text{Fe}_3\text{O}_4$  nanoparticles with a desired concentration were synthesized by the hydrolysis of a mixture of iron (II) and iron (III) salts at a ratio of 1 : 2 (0.108–0.86 g  $\text{FeSO}_4 \cdot 7\text{H}_2\text{O}$  and 0.294–2.35 g  $\text{FeCl}_3 \cdot 6\text{H}_2\text{O}$ ) in an ammonium hydroxide solution at 60°C. The suspension was heated in a water bath up to 80°C and stirred for 0.5 h. Cooling of the suspension was carried out at room temperature with constant vigorous stirring for 1 h. To attach a monomer to the surface,  $\text{Fe}_3\text{O}_4$  nanoparticles were filtered and washed with distilled water for the removal of the residual reagents until a neutral reaction of a filtrate was achieved; then they were immediately (without prior drying) added to the ADMPhH acetonitrile solution of the desired concentration. The process was run at 60°C with constant vigorous stirring for 1 h. Cooling of the suspension was carried out with stirring at room temperature for 1 h. The obtained  $\text{Fe}_3\text{O}_4/\text{ADMPhH}$  suspension was stirred in an ultrasonic bath at room temperature for 0.5 h. Then, to carry out in situ oxidative polymerization of ADMPhH at the surface of  $\text{Fe}_3\text{O}_4$  nanoparticles, an aqueous ammonium persulfate solution was added dropwise to the  $\text{Fe}_3\text{O}_4/\text{ADMPhH}$  suspension in acetonitrile thermostatted at 15°C with constant stirring. The proportion between the volumes of organic and water phases was 1 : 1 ( $V_{\text{tot}} = 60$  mL). The reaction temperature was maintained at no higher than 15°C. The polymerization reaction was conducted with constant vigorous stirring for 4 h. After the end of the synthesis, the reaction mixture was precipitated in a five-fold excess of distilled water. The final product was filtered, repeatedly washed with distilled water to remove residual reagents, and dried under vacuum above KOH until the mass became constant. The  $\text{Fe}_3\text{O}_4/\text{PAMMPh}$  yield is 1.18 g at an iron content of Fe = 50.4% (according to the AAS data) (Table 1). The oxidative polymerization of ADMPhH at the surface of  $\text{Fe}_3\text{O}_4$  nanoparticles can also be carried out in a DMFA aqueous solution.

The metal content in the  $\text{Fe}_3\text{O}_4/\text{PAMMPh}$  nanocomposite was determined quantitatively by atomic absorption spectrometry on an AAS 30 spectrophotometer (Carl Zeiss JENA) (Table 1). The error of determination of the Fe content was  $\pm 1.0\%$ .

The IR spectra of the samples were recorded on an IFS 66v Fourier transform IR spectrometer in the range of 4000–400  $\text{cm}^{-1}$ . The samples were prepared in the form of tablets pressed with KBr.

X-ray structural investigations were carried out at room temperature on a Difrei-401 X-ray diffractometer with Bragg–Brentano geometry in  $\text{Cr } K_\alpha$  radiation at  $\lambda = 0.229$  nm. Using the results of X-ray structural

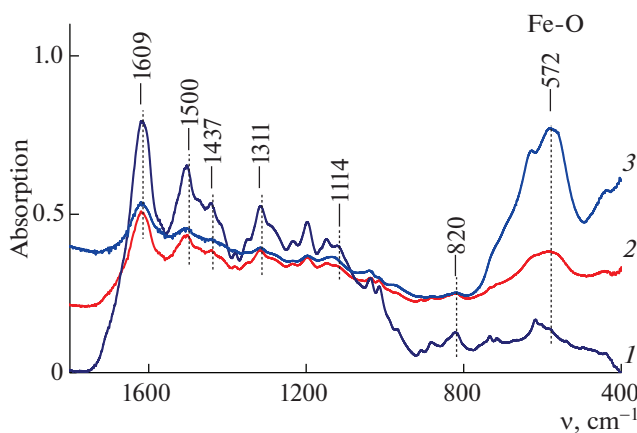


**Fig. 1.** (Color online) IR spectra of (1) the PAMMPh and the nanocomposite  $\text{Fe}_3\text{O}_4/\text{PAMMPh}$  obtained at  $[\text{Fe}] = 21.2$  (2) and 50.4% (3).

analysis, the size distribution of the coherent scattering regions (CSRs) of crystallites [28] in  $\text{Fe}_3\text{O}_4$  nanoparticles was calculated.

Electron microscopy investigations were conducted on a LEO912 AB OMEGA transmission electron microscope and a Supra 25 field-emission scanning electron microscope (Zeiss). The resolution in the obtained images is 1 to 2 nm. The size of nanoparticles was determined using the EsiVision program.

To measure the magnetic characteristics of the systems, a vibrating-coil magnetometer was employed [29]. The measurements of the magnetization were performed depending on the magnetic field value, and the magnetic characteristics of the samples were determined at room temperature.

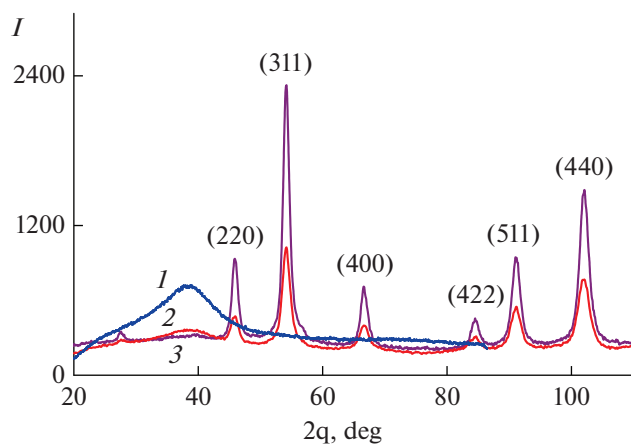


**Fig. 2.** (Color online) XRD patterns of (1) the PAMMPh and the nanocomposite  $\text{Fe}_3\text{O}_4/\text{PAMMPh}$  obtained at  $[\text{Fe}] = 21.2$  (2) and 50.4% (3).

Thermal analysis was carried out on a TGA/DSC1 instrument (Mettler Toledo) in a dynamic mode in the temperature range of 30–1000°C in air and in an argon flow. The weight amount of the samples was 100 mg, the heating rate was 10°C/min, and the argon flow rate was 10 mL/min. As a reference sample, calcined aluminum oxide was used. The samples were analyzed in an  $\text{Al}_2\text{O}_3$  crucible.

DSC analysis was performed on a DSC823 calorimeter (Mettler Toledo). The samples were heated at a rate of 10°C/min a nitrogen atmosphere at the nitrogen flow rate of 70 mL/min. The results were treated using the STARE service software delivered with the instrument.

## RESULTS AND THEIR DISCUSSION

A hybrid nanomaterial  $\text{Fe}_3\text{O}_4/\text{PAMMPh}$  is obtained under the conditions of in situ oxidative polymerization of ADMPhH in the presence of  $\text{Fe}_3\text{O}_4$  nanoparticles. The formation of the hybrid dispersed  $\text{Fe}_3\text{O}_4/\text{PAMMPh}$  nanomaterial includes the synthesis of  $\text{Fe}_3\text{O}_4$  nanoparticles by means of hydrolysis of a mixture of iron (II) and iron (III) salts at a ratio of 1 : 2 in an ammonium hydroxide solution [30], the attachment of the monomer to the surface of priorly obtained magnetite nanoparticles introduced into the reaction medium of nanocomposite synthesis, and subsequent in situ polymerization in the presence of ammonium persulfate as an oxidizing agent.

The formation of the nanocomposite material  $\text{Fe}_3\text{O}_4/\text{PAMMPh}$  is confirmed by techniques such as Fourier transform IR spectroscopy, X-ray structural investigations, AAS, and transmission (TEM) and field-emission scanning electron microscopy (FE-SEM).

Figure 1 shows the FTIR spectra of PAMMPh and a nanocomposite based on it. The comparison of the

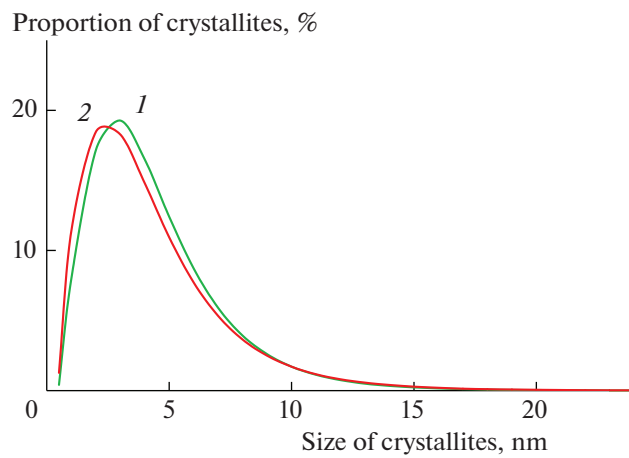


**Fig. 3.** (Color online) Size distribution of  $\text{Fe}_3\text{O}_4$  crystallites in the nanocomposite  $\text{Fe}_3\text{O}_4/\text{PAMMPh}$  obtained at  $[\text{Fe}] = 21.2$  (1) and 50.4% (2).

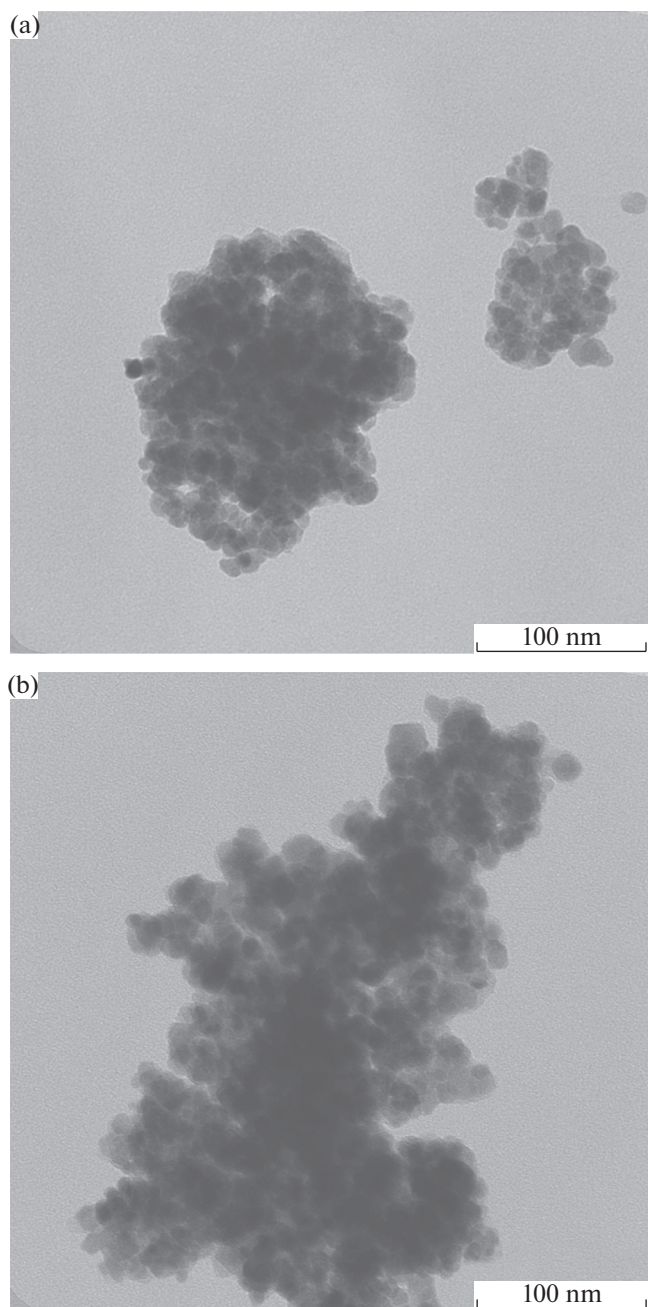


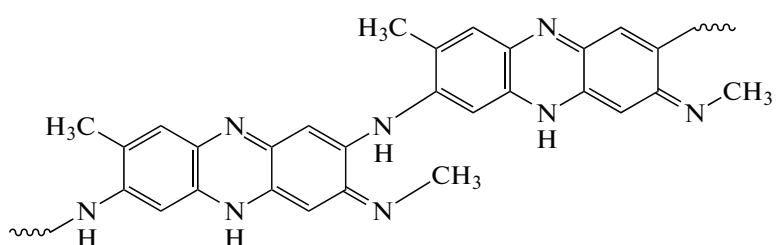
**Fig. 4.** TEM images of the nanocomposite  $\text{Fe}_3\text{O}_4/\text{PAMMPh}$  obtained at  $[\text{Fe}] = 21.2$  (a) and 50.4% (b).

IR spectra of the polymer and the nanocomposite revealed that, in the IR spectra of  $\text{Fe}_3\text{O}_4/\text{PAMMPh}$  all

main bands characteristic of the PAMMPh chemical structure persist. It is established that, as with PAMMPh [25], in the nanocomposite, the chain propagation proceeds via the addition of C–N between 3-amino groups and the *para* position of phenyl rings relative to nitrogen with the simultaneous splitting out of a  $\text{Cl}^-$  anion and a methyl group from the 7-dimethylamino group. The absorption band at  $820 \text{ cm}^{-1}$ , as well as the bands at  $1287$  and  $1114 \text{ cm}^{-1}$ , are due to the out-of-plane deformation vibrations of the  $\delta_{\text{C}-\text{H}}$  bonds of the 1,2,4,5-substituted benzene ring [31–33]. The absorption bands at  $806$ ,  $731$ , and  $714 \text{ cm}^{-1}$  relate to the out-of-plane deformation vibrations of the  $\delta_{\text{C}-\text{H}}$  bonds of a trisubstituted benzene ring of the terminal groups. The intense bands at  $1609$  and  $1500 \text{ cm}^{-1}$  correspond to the stretching vibrations of the  $\nu_{\text{C}-\text{C}}$  bonds in aromatic rings [25]. The absorption bands at  $1342$ ,  $1311$ , and  $1226 \text{ cm}^{-1}$  relate to the stretching vibrations of the  $\nu_{\text{C}-\text{N}}$  bonds [25]. A triplet in the vicinity of  $2900 \text{ cm}^{-1}$  is that of the stretching vibrations of the  $\nu_{\text{C}-\text{H}}$  bonds in  $-\text{CH}_3$  [34, 35]. This is corroborated by the presence of a band at  $1437 \text{ cm}^{-1}$  from the deformation vibrations of the  $\delta_{\text{C}-\text{H}}$  bonds in  $-\text{CH}_3$  [25].

In the IR spectra of the nanocomposite (Fig. 1), an absorption band in the vicinity of  $572 \text{ cm}^{-1}$  is present along with a band at  $433 \text{ cm}^{-1}$ , which both characterize the stretching vibrations of the  $\nu_{\text{Fe}-\text{O}}$  bond of magnetite. It is worthy to note that the absorption bands of the stretching vibrations of the  $\text{Fe}-\text{O}$  bond in magnetite lie in the vicinity of  $480$  and  $440 \text{ cm}^{-1}$  [36]. A strong shift to a shorter wavelength range is evidence of the interaction between magnetite and the polymer functional groups. An increase in the  $\text{Fe}_3\text{O}_4$  content of the nanocomposite leads to a considerable growth in the intensity of the band at  $572 \text{ cm}^{-1}$ .

Therefore, according to the results of Fourier transform IR spectroscopy, a polymer matrix (poly-3-amino-7-methylamine-2-methylphenazine) has the following chemical structure:



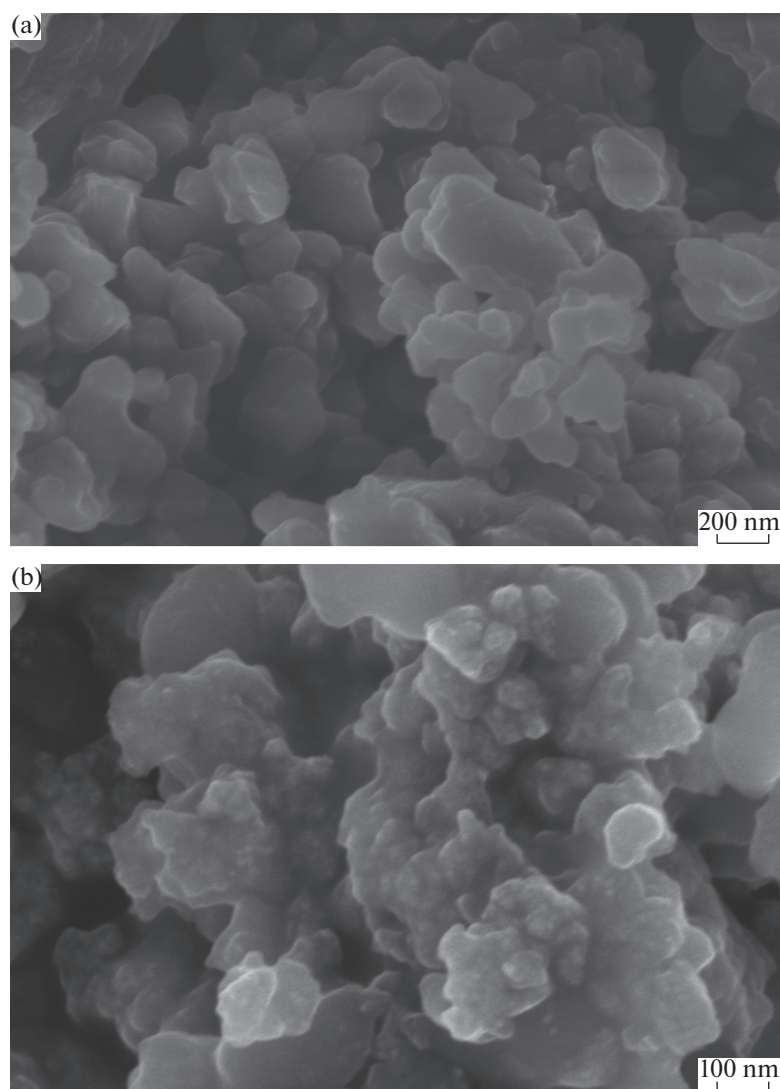


**Fig. 5.** FE-SEM images of the PAMMPh (a) and the nanocomposite Fe<sub>3</sub>O<sub>4</sub>/PAMMPh obtained at [Fe] = 21.2% (b).

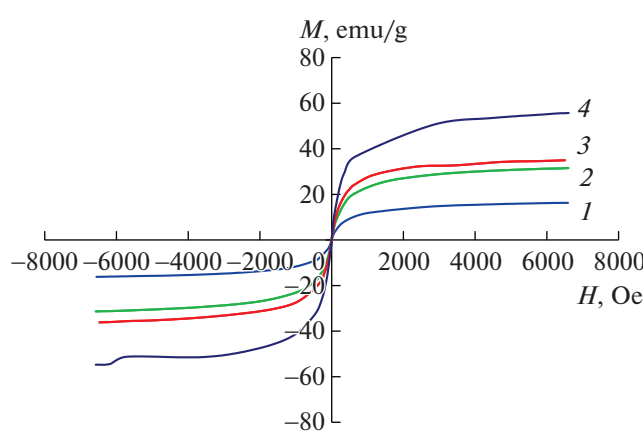


**Fig. 6.** (Color online) Magnetization of the nanocomposite Fe<sub>3</sub>O<sub>4</sub>/PAMMPh versus the applied magnetic field at room temperature, where the Fe<sub>3</sub>O<sub>4</sub>/PAMMPh is obtained at [Fe] = 21.2 (1), 33.5 (2), 44.5 (3), and 50.4% (4).

PAMMPh is a semiladder heterocyclic polymer containing nitrogen atoms involved in the common polyconjugated system.

The formation of Fe<sub>3</sub>O<sub>4</sub> nanoparticles is confirmed by XRA. The only metal-containing phase in the nanocomposite composition is the phase Fe<sub>3</sub>O<sub>4</sub>. In the diffraction patterns of the nanocomposite, the reflection peaks of Fe<sub>3</sub>O<sub>4</sub> in the vicinity of the scattering angles  $2\theta = 46.1^\circ, 54.2^\circ, 66.9^\circ, 84.8^\circ, 91.2^\circ$ , and  $102.2^\circ$  (Cr  $K_\alpha$  radiation) are clearly identifiable (Fig. 2) [22, 23]. All these diffraction peaks belong to the Fe<sub>3</sub>O<sub>4</sub> cubic structure (JCPDS 19-0629); the corresponding Miller indices are (220), (311), (400), (422), (511), and (440) [37]. The size distribution of CSRs in Fe<sub>3</sub>O<sub>4</sub> nanoparticles was calculated from the XSA results (Fig. 3). About 90 to 95% of Fe<sub>3</sub>O<sub>4</sub> crystallites are up to 8 nm in size. According to the TEM

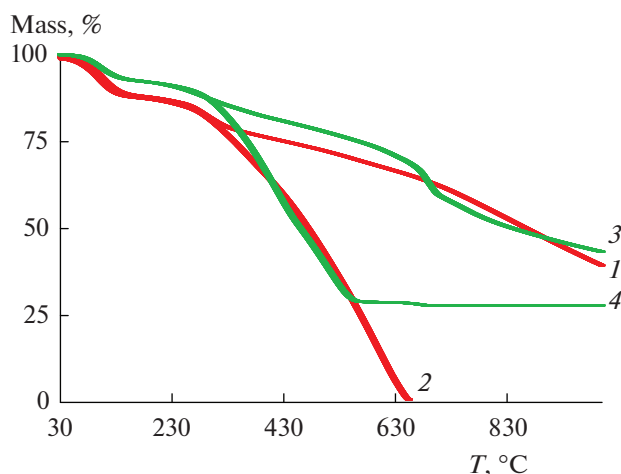


**Fig. 7.** (Color online) Decrease in the mass of (1, 2) the PAMMPh and the nanocomposite  $\text{Fe}_3\text{O}_4/\text{PAMMPh}$  obtained at  $[\text{Fe}] = 21.2\%$  (3, 4) upon heating to  $1000^\circ\text{C}$  at a rate of  $10^\circ\text{C}/\text{min}$  (1, 3) in an argon flow and (2, 4) in air.

and FE-SEM results,  $\text{Fe}_3\text{O}_4$  nanoparticles have sizes of  $4 < d < 11 \text{ nm}$  (Figs. 4, 5). According to the AAS data, the iron content is  $[\text{Fe}] = 21.2\text{--}50.4\%$  depending on the synthetic conditions (Table 1).

The magnetic properties of the  $\text{Fe}_3\text{O}_4/\text{PAMMPh}$  nanomaterial are investigated and the values of its main magnetic characteristics are determined. The dependence of the magnetization on the value of the applied magnetic field at room temperature is shown in Fig. 6. The effect of the iron concentration on the magnetic characteristics of the  $\text{Fe}_3\text{O}_4/\text{PAMMPh}$  nanomaterial was investigated. The saturation magnetization  $M_s$  depends on the iron concentration and reaches  $55.7 \text{ emu/g}$  at  $[\text{Fe}] = 50.4\%$  (Table 1). The squareness ratio of the hysteresis loop is  $k_s = M_R/M_s \sim 0$ , which indicates that the behavior of the hybrid nanomaterial is superparamagnetic [29, 38], caused by small sizes and high degree of dispersion of magnetic nanoparticles. The values  $M_R/M_s$  are typical of single-axis single-domain particles. For  $\text{Fe}_3\text{O}_4$ , the critical size of the transition to a single-domain state is  $128 \text{ nm}$  [29, 38].

**Table 2.** Thermal properties of materials

Characteristics	PAMMPh	$\text{Fe}_3\text{O}_4/\text{PAMMPh}$
* $T_{5\%}$ , $^\circ\text{C}$	87/96	114/116
** $T_{25\%}$ , $^\circ\text{C}$	342/434	365/565
*** $T_{50\%}$ , $^\circ\text{C}$	474/865	460/841
****Остаток, %	0/39	28/43

\* $T_{5\%}$ , \*\* $T_{25\%}$ , and \*\*\* $T_{50\%}$  correspond to the 5, 25, and 50% mass loss (air/Ar).

\*\*\*\*Residue at  $1000^\circ\text{C}$  (air/Ar).  $[\text{Fe}_3\text{O}_4] = 27.6\%$ .

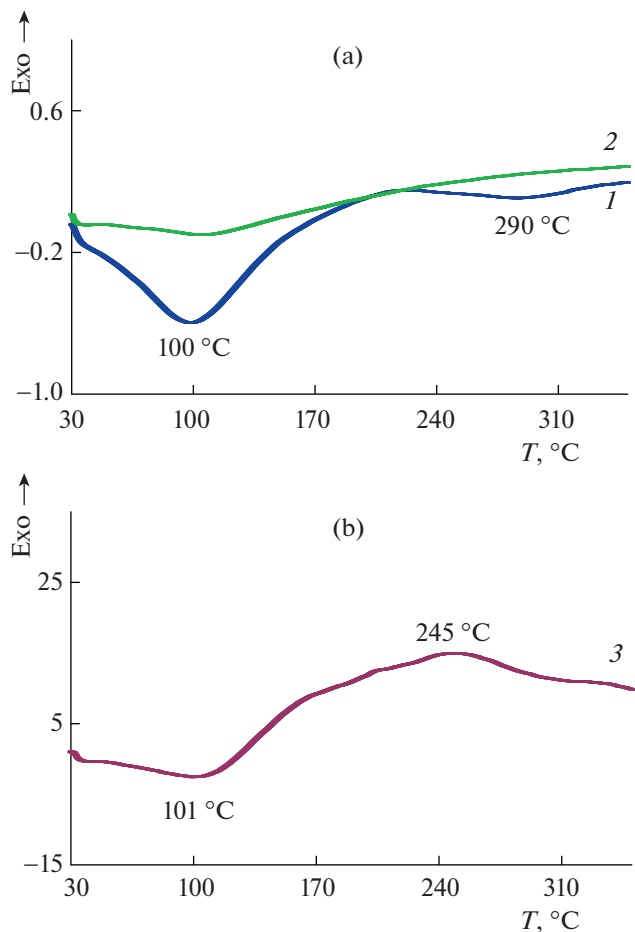


**Fig. 8.** (Color online) DSC thermograms of (1, 2) the nanocomposite  $\text{Fe}_3\text{O}_4/\text{PAMMPh}$  and (3) PAMMPh upon heating to  $350^\circ\text{C}$  in an argon flow at a rate of  $10^\circ\text{C}/\text{min}$  (1 and 3 indicate the first heating and 2 indicates the second heating).

The thermal stability of the  $\text{Fe}_3\text{O}_4/\text{PAMMPh}$  nanocomposite was investigated by TGA and DSC techniques. Figure 7 illustrates the temperature dependence of the decrease in the mass of the  $\text{Fe}_3\text{O}_4/\text{PAMMPh}$  nanocomposite in comparison with that of PAMMPh upon heating to  $1000^\circ\text{C}$  in an argon flow and in air. According to the AAS data, the content  $[\text{Fe}_3\text{O}_4] = 27.6\%$ . Table 2 presents the main thermal characteristics of the materials. As is seen from Fig. 7, the character of the curves showing the mass loss of the samples remains unchanged up to  $320^\circ\text{C}$ . In the process, the mass loss at low temperatures is due to the removal of moisture, which is confirmed by the DSC data (Fig. 8). In the DSC thermograms of the nanocomposite and the polymer, there is an endothermic peak at  $\sim 100^\circ\text{C}$ . With the second heating, this peak is absent. The exothermic peak observed in the polymer DSC thermogram at  $245^\circ\text{C}$  cannot be due to the processes of melting or cross-linking, because, according to the XRA data, PAMMPh is an amor-

phous polymer (Fig. 2) and, in the indicated temperature range, in the TGA cumulative curves, small mass loss is observed.

In the  $\text{Fe}_3\text{O}_4/\text{PAMMPh}$  hybrid nanomaterial, the absence of mass loss in air at a temperature higher than 570°C is due to the complete thermal-oxidative destruction of the polymer matrix. After the destruction of the polymer matrix, magnetite is left. At 1000°C, the residue comprises 28%, which corresponds to the  $\text{Fe}_3\text{O}_4$  content of the nanocomposite of  $[\text{Fe}_3\text{O}_4] = 27.6\%$ , as the AAS data show.

In an inert medium, at higher than 320°C, the loss of the mass of the samples takes place gradually. In the  $\text{Fe}_3\text{O}_4/\text{PAMMPh}$  nanocomposite, at 1000°C, the residue is 43% and, in the PAMMPh, the residue is 39%.

## CONCLUSIONS

Under the conditions of in situ oxidative polymerization, in an acetonitrile aqueous solution in the presence of magnetite nanoparticles introduced into the reaction medium beforehand, a hybrid dispersed magnetic nanomaterial  $\text{Fe}_3\text{O}_4/\text{PAMMPh}$  is obtained for the first time.  $\text{Fe}_3\text{O}_4$  nanoparticles have sizes of  $4 < d < 11 \text{ nm}$ . The saturation magnetization  $M_s$  depends on the iron concentration and is 16.3–55.7 emu/g at  $[\text{Fe}] = 21.2\text{--}50.4\%$ . The squareness ratio of the hysteresis loop is  $k_s = M_R/M_S \sim 0$ , which indicates that the behavior of the hybrid nanomaterial is superparamagnetic. The nanocomposite loses half of its initial mass at 460°C in air and at 841°C in an inert medium. At 1000°C, the residue is 43%. These hybrid nanomaterials are rather attractive for modern technologies and can be applied in the creation of electromagnetic screens and contrast materials for magnetic resonance tomography and as materials absorbing electromagnetic radiation in different wavelength ranges.

## ACKNOWLEDGMENTS

The work was carried out under the state assignment of the Topchiev Institute of Petrochemical Synthesis of the Russian Academy of Sciences. In the study, equipment of the New Petrochemical Processes, Polymer Composites, and Adhesives shared facilities was employed.

## REFERENCES

- R. M. Cornel and U. Schwertmann, *The Iron Oxides: Structure, Properties, Reactions, Occurrences and Uses* (VCH, New York, 1996).
- D. Y. Godovsky, "Device applications of polymer-nanocomposites," *Adv. Polym. Sci.* **153** (15), 163–205 (2000).
- G. P. Karpacheva, "Hybrid magnetic nanocomposites including polyconjugated polymers," *Polym. Sci., Ser. C* **58**, 131–146 (2016).
- X. Lu, Y. Yu, L. Chen, H. Mao, H. Gao, J. Wang, W. Zhang, and Y. Wey, "Aniline dimmer-COOH assisted preparation of well-dispersed polyaniline- $\text{Fe}_3\text{O}_4$  nanoparticles," *Nanotecnology* **16**, 1660–1665 (2005).
- D. Chao, X. Lu, J. Chen, W. Zhang, and Y. Wei, "Anthranilic acid assisted preparation of  $\text{Fe}_3\text{O}_4$ -poly(aniline-co-o-anthranilic acid) nanoparticles," *J. Appl. Polym. Sci.* **102**, 1666–1671 (2006).
- J. Du, Q. Peng, R. Qiao, W. Chen, C. Xu, Z. Shuai, and M. Gao, "Polyaniline/ $\text{Fe}_3\text{O}_4$  nanoparticle composite: synthesis and reaction mechanism," *J. Phys. Chem. B* **113**, 5052–5058 (2009).
- G. Qiu, Q. Wang, and M. Nie, "Polyaniline/ $\text{Fe}_3\text{O}_4$  magnetic nanocomposite prepared by ultrasonic irradiation," *J. Appl. Polym. Sci.* **102**, 2107–2111 (2006).
- A. Khan, A. S. Aldwayan, M. Alhoshan, and M. Alsalhi, "Synthesis by in situ chemical oxidative polymerization and characterization of polyaniline/iron oxide nanoparticle composite," *Polym. Int.* **59**, 1690–1694 (2010).
- S. S. Umare and B. H. Shambharkar, "Synthesis, characterization, and corrosion inhibition study of polyaniline- $\alpha\text{-Fe}_2\text{O}_3$  nanocomposite," *J. Appl. Polym. Sci.* **127**, 3349–3355 (2013).
- N. N. Mallikarjuna, S. K. Manohar, P. V. Kulkarni, A. Venkataraman, and T. M. Aminabhavi, "Novel high dielectric constant nanocomposites of polyaniline dispersed with  $\gamma\text{-Fe}_2\text{O}_3$  nanoparticles," *J. Appl. Polym. Sci.* **97**, 1868–1874 (2005).
- M. Bhaumik, T. Y. Leswifi, A. Maity, V. V. Srinivasu, and M. S. Onyango, "Removal of fluoride from aqueous solution by polypyrrole/ $\text{Fe}_3\text{O}_4$  magnetic nanocomposite," *J. Hazard. Mater.* **186**, 150–159 (2011).
- M. Jokar, R. Foroutani, M. H. Safaralizadeh, and K. Farhadi, "Synthesis and characterization of polyaniline/ $\text{Fe}_3\text{O}_4$  magnetic nanocomposite as practical approach for fluoride removal process," *Ann. Res. Rev. Biol.* **4**, 3262–3273 (2014).
- B. H. Shambharkar and S. S. Umare, "Production and characterization of polyaniline/ $\text{Co}_3\text{O}_4$  nanocomposite as a cathode of zn-polyaniline battery," *Mater. Sci. Eng. B* **175**, 120–128 (2010).
- A. Chen, H. Wang, B. Zhao, J. Wang, and X. Li, "Preparation and characterization of  $\text{Fe}_3\text{O}_4$ /polypyrrole (PPy) composites," *Acta Mater. Compos. Sin.* **21**, 157–160 (2004).
- L. Li, J. Jiang, and F. Xu, "Novel polyaniline- $\text{LiNi}_{0.5}\text{La}_{0.02}\text{Fe}_{1.98}\text{O}_4$  nanocomposites prepared via an in situ polymerization," *Eur. Polym. J.* **42**, 2221–2227 (2006).
- L. Li, J. Jiang, and F. Xu, "Synthesis and ferrimagnetic properties of novel Sm-substituted LiNi ferrite-polyaniline nanocomposite," *Mater. Lett.* **61**, 1091–1096 (2007).
- G. D. Prasanna, H. S. Jayanna, and V. Prasad, "Preparation, structural, and electrical studies of polyaniline/Zn $\text{Fe}_2\text{O}_4$  nanocomposites," *J. Appl. Polym. Sci.* **120**, 2856–2862 (2011).

18. J. C. Aphesteguy and S. E. Jacobo, "Composite of polyaniline containing iron oxides," *Phys. B* (Amsterdam, Neth.) **354**, 224–227 (2004).
19. M. Wan and J. Li, "Synthesis and electrical-magnetic properties of polyaniline composites," *J. Polym. Sci., A* **36**, 2799–2805 (1998).
20. Z. Zhang and M. Wan, "Nanostructures of polyaniline composites containing nano-magnet," *Synth. Met.* **132**, 205–212 (2003).
21. G. P. Karpacheva and S. Zh. Ozkan, "Dispersed nano-composite magnetic material and method of its obtaining," RF Patent No. 2426188, Byull. Izobret. No. 22 (2011).
22. I. S. Eremeev, S. Zh. Ozkan, G. P. Karpacheva, and G. N. Bondarenko, "Hybrid dispersed magnetic nanomaterial based on polydiphenylamine-2-carboxylic acid and  $\text{Fe}_3\text{O}_4$ ," *Nanotechnol. Russ.* **9**, 38–44 (2014).
23. G. P. Karpacheva, S. Zh. Ozkan, I. S. Eremeev, G. N. Bondarenko, E. L. Dzidziguri, and P. A. Chernavskii, "Synthesis of hybrid magnetic nanomaterial based on polydiphenylamine-2-carboxylic acid and  $\text{Fe}_3\text{O}_4$  in the interfacial process," *Eur. Chem. Bull.* **3**, 1001–1007 (2014).
24. S. Zh. Ozkan, G. P. Karpacheva, E. L. Dzidziguri, P. A. Chernavskii, G. N. Bondarenko, and G. V. Pankina, "Formation features of hybrid magnetic materials based on polyphenoxazine and magnetite nanoparticles," *J. Res. Updates Polym. Sci.* **5**, 137–148 (2017).
25. S. Zh. Ozkan, G. P. Karpacheva, G. N. Bondarenko, and Yu. G. Kolyagin, "Polymers based on 3-amine-7-dimethylamine-2-methylphenazine hydrochloride: synthesis, structure, and properties," *Polym. Sci., Ser. B* **57**, 106–115 (2015).
26. Yu. V. Karyakin and I. I. Angelov, *Pure Chemical Reagents* (Khimiya, Moscow, 1974) [in Russian].
27. S. Zh. Ozkan and G. P. Karpacheva, "Metal-polymer nanocomposite magnetic material based on poly-3-amine-7-methylamine-2-methylphenazine and  $\text{Fe}_3\text{O}_4$  nanoparticles and method of its production," RU Patent No. 2637333 C2, Byull. Izobret. No. 34 (2017).
28. E. L. Dzidziguri, "Dimensional characteristics of nanopowders," *Nanotechnol. Russ.* **4**, 857–870 (2009).
29. P. A. Chernavskii, G. V. Pankina, and V. V. Lunin, "Magnetometric methods of investigation of supported catalysts," *Russ. Chem. Rev.* **80**, 579–604 (2011).
30. R. Massart, "Preparation of aqueous magnetic liquids in alkaline and acidic media," *IEEE Trans. Magn.* **17**, 1247–1248 (1981).
31. J. Tang, X. Jing, B. Wang, and F. Wang, "Infrared spectra of soluble polyaniline," *Synth. Met.* **24**, 231–238 (1988).
32. M. Trchova, J. Prokes, and J. Stejskal, "Infrared spectroscopic study of solid-state protonation and oxidation of polyaniline," *Synth. Met.* **101**, 840–841 (1999).
33. N. V. Bhat, D. T. Seshadri, and R. S. Phadke, "Simultaneous polymerization and crystallization of aniline," *Synth. Met.* **130**, 185–192 (2002).
34. P. S. Rao, S. Subrahmanyam, and D. N. Sathyaranayana, "Inverse emulsion polymerization: a new route for the synthesis of conducting polyaniline," *Synth. Met.* **128**, 311–316 (2002).
35. Z. Ping, "In situ FTIR-attenuated total reflection spectroscopic investigations on the base-acid transitions of polyaniline. base-acid transition in the emeraldine form of polyaniline," *J. Chem. Soc., Faraday Trans.* **92**, 3063–3067 (1996).
36. M. I. Ivanovskaya, A. I. Tolstik, D. A. Kotikov, and V. V. Pankov, "The structural characteristics of Zn–Mn ferrite synthesized by spray pyrolysis," *Russ. J. Phys. Chem. A* **83**, 2081–2086 (2009).
37. A. Yu. Soloveva, Y. V. Ioni, and S. P. Gubin, "Synthesis of  $\text{Fe}_3\text{O}_4$  nanoparticles on the surface of graphene," *Mendeleev Commun.* **26**, 38–39 (2016).
38. S. P. Gubin, Yu. A. Koksharov, G. B. Khomutov, and G. Yu. Yurkov, "Magnetic nanoparticles: preparation, structure and properties," *Russ. Chem. Rev.* **74**, 489–520 (2005).

*Translated by Z. Smirnova*

SPELL: OK